Revision 3

Word Count: 7217

Element mobility and oxygen isotope systematics during submarine alteration of basaltic glass

Miaohong He [1, 2*], Shudi Zhang [3, 4], Le Zhang [1, 2], Fan Yang [1, 2], Yanqiang Zhang [1, 2], Xiaolong Huang [1, 2], Gangjian Wei [1, 2]

[1] State Key Laboratory of Isotope Geochemistry, Guangzhou Institute of Geochemistry, Chinese Academy of Sciences, Guangzhou 510640, China

[2] CAS Center for Excellence in Deep Earth Science, Guangzhou, 510640, China

[3] Department of Public Health and Medical Technology, Xiamen Medical College, Xiamen 361023, Fujian, China

[4] Engineering Research Center of Natural Cosmeceuticals College of Fujian Province, Xiamen Medical College, Xiamen 361023, Fujian, China

*Corresponding author: Miaohong He

Tel: 86-20-85290501

E-mail: mhhe@gig.ac.cn

Abstract

Studies of the submarine alteration of basaltic glass may improve the understanding of crust–seawater interactions and the oceanic elemental cycle. Natural alteration processes such as the palagonitization of basaltic glass are complex, and their elucidation is crucial to the understanding of fluid–rock interactions. This study involves major and trace element and isotope mapping of a submarine-altered basaltic glass grain, and reveals sequential development of alteration textures toward the grain core through the transition between unaltered glass and palagonite. The conversion from basaltic glass to palagonite in a low-temperature submarine environment results in enrichment in B, Rb, K, Li, H_2O, U, Nb, Th, Ti, Cu, Ta, Zr, Hf, Ni, Sc, Fe, Cr, Pb, and Zn; and depletion in Si, Mg, Al, Sr, Na, Co, rare-earth elements, Ca, P, and V (in order of decreasing distribution coefficient). The glass–palagonite interface region has the highest high field strength element (HFSE) and Fe–Ti contents, but the lowest Mg content, indicating that the Fe–Ti phases that host HFSE were precipitated first during initial palagonitization. At the same time an inferred exchange of oxygen occurred, based on variation in $\delta^{18}O$, with values increasing from basaltic glass to palagonite. However, initial palagonite compositions were affected by subsequent precipitation and/or incorporation/adsorption of additional compounds such as $Mg(OH)_2$ scavenged from pore water.

Keywords: basaltic glass; palagonite; alteration; elemental imaging; oxygen isotope

1. Introduction

Basaltic glass is the most abundant unstable, highly reactive solid on the seafloor (Staudigel and Hart 1983; Utzmann et al. 2002; Walton et al. 2005), and its alteration attracts increasing attention within geochemistry and materials science. Study of basaltic glass alteration is important for improving the understanding of oceanic crust–seawater interactions (Utzmann et al. 2002), for determining the composition of groundwater in basaltic terrains such as Iceland (Gislason and Eugster 1987), and in calculating the flux of materials in geochemical cycles involving seawater and oceanic crust. Basaltic glass is also considered a natural analogue of glass used for containment of radioactive waste, owing to their similar chemical compositions (Crovisier et al. 2003; Daux et al. 1994; Gin et al. 2015a; Gin et al. 2013; Grambow et al. 1985; Lutze et al. 1985; Techer et al. 2001b), and it provides a means of assessing theoretical models of the long-term safety of nuclear waste disposal in borosilicate glass (Crovisier et al. 2003; Jantzen and Plodinec 1984; Techer et al. 2000; Techer et al. 2001b). The alteration of glass may also provide guidance for archaeologists during heritage conservation (Saheb et al. 2015).

Palagonitization is a geochemical alteration process common to basaltic glass (Jercinovic et al. 1990; Pauly et al. 2011; Stroncik and Schmincke 2002; Walton and Schiffman 2003), but its controls and mechanism are not fully understood (Drief and Schiffman 2004; Pauly et al. 2011). Palagonite is generally considered the initial metastable alteration product of volcanic glass (Jercinovic et al. 1990; Stroncik and

Schmincke 2002; Stroncik and Schmincke 2001), and usually occurs on exposed glass surfaces such as grain peripheries, vesicle walls, and along fractures (Jercinovic et al. 1990; Stroncik and Schmincke 2001; Techer et al. 2001b; Walton and Schiffman 2003). An investigation of compositional variations during basaltic glass alteration to palagonite may elucidate the alteration process. Traditional bulk analysis techniques have high precision and accuracy, and are easily applied to the determination of major and trace element compositions of altered glass, but cannot completely differentiate unaltered and altered material whose thickness are in the range of micrometers (Ailin-Pyzik and Sommer 1981; Hart 1970; Hart 1969). Differentiation may be achieved by *in situ* elemental analysis procedures with high spatial resolution, such as electron microprobe analysis (EPMA), micro-X-ray fluorescence spectroscopy (XRF), and laser ablation–inductively coupled plasma–mass spectrometry (LA–ICP–MS). The use of LA–ICP–MS allows simultaneous quantitative analyses of major and trace elements (including elements with low atomic mass) in glass and palagonite, with low detection limits (in favorable cases to parts per trillion, ppt) (Belza et al. 2015; Drief and Schiffman 2004; Knowles et al. 2013; Nikitczuk et al. 2016; Pauly et al. 2011; Thorseth et al. 1991; Utzmann et al. 2002; Walton et al. 2005). Two-dimensional elemental imaging allows observation of variations between pristine glass and its alteration phase (palagonite), while clearly revealing fine spatial compositional changes. Qualitative elemental imaging of altered glass has been reported in previous studies, which have focused on the

compositional differences of certain elements between glass and alteration phases (palagonite, smectite, or zeolite) (Belza et al. 2015; Knowles et al. 2013; Stroncik and Schmincke 2001; Utzmann et al. 2002). However, there has been little study of the overall process from initial precipitation to aged palagonite (before crystallization with smectite), which is of importance for comprehensive understanding of glass alteration.

In this study, major and trace element imaging by LA–ICP–MS and oxygen isotope analyses by secondary ion mass spectrometry (SIMS) were undertaken for an individual submarine-altered basaltic glass grain. Chemical mobility and oxygen isotopic features during alteration from basaltic glass to palagonite were recorded visually and quantitatively and focused on the glass–palagonite interface, which is critical to elucidating the process of glass alteration.

2. Experimental

2.1 Sample descriptions

The studied sample was collected from a >2500-m-deep basin in the South China Sea, at site U1434 of the 2014 International Ocean Discovery Program Expedition 349, near Fossil Spreading Ridge in the southwest sub-basin at 278.3–308.7 meters below seafloor (Fig. 1), and is dated at *ca* 17.3 Ma (Zhang et al. 2018a). The geological setting has been described previously by Li et al. (2015a; 2014). The sample includes a black core of mid-ocean-ridge basalt (MORB) glass, with a brown palagonite rim (Fig. 2) resulting

This is the peer-reviewed, final accepted version for American Mineralogist, published by the Mineralogical Society of America.
The published version is subject to change. Cite as Authors (Year) Title. American Mineralogist, in press.
DOI: https://doi.org/10.2138/am-2021-7831. http://www.minsocam.org/

from low temperature (<5°C) alteration (Li et al. 2015a). The interface is markedly optically different from either glass or outer palagonite crust (Fig. 2b). Palagonite thickness is generally considered time-dependent (as the alteration reaction proceeds), and is often used as a chronological indicator in both archeology and geology (Crovisier et al. 1992; Grambow et al. 1985; Morgenstein and Riley 1974; Stroncik and Schmincke 2002; Techer et al. 2001a; Techer et al. 2001b). The thickness of the individual grain here varies between 134 and 660 μm, which yields a mean alteration rate of about 1.6×10^{-7} $g.m^{-2}.d^{-1}$ according to the calculation proposed by Parruzot et al (2015).

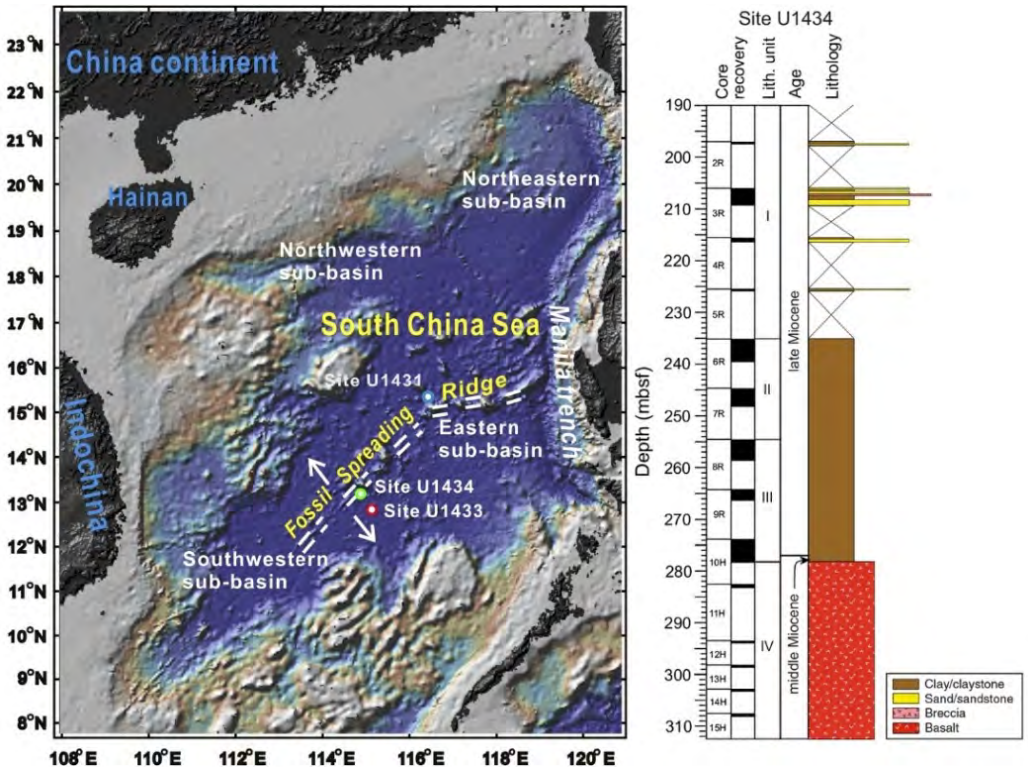

Fig. 1 Geological setting of the South China Sea, showing the location of the U1434 sampling site and the lithostratigraphic details of the core (modified from Zhang et al.

113 (2018) and Li et al.(2015)).

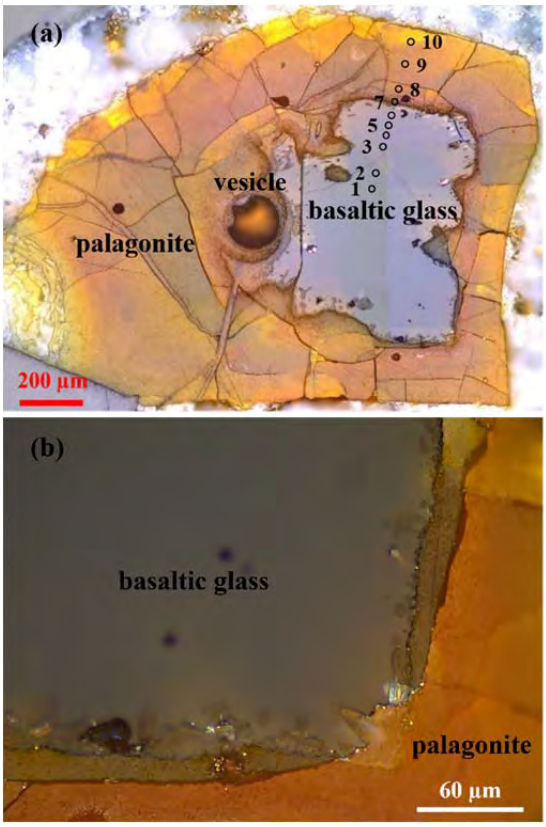

114

115 Fig. 2 (a) Photomicrograph in plane polarized transmitted light of the altered basaltic
116 glass sample showing brown palagonite alteration rims. Numbered circles indicate
117 analysis spots for SIMS oxygen isotope, H_2O, and EPMA major element analyses. The
118 sample vesicle is empty. (b) Photomicrograph showing a closer view of the interface
119 between palagonite and glass.

120

121 **2.2 Instrumental and analytical procedures**

122 **2.2.1 Elemental imaging by LA–ICP–MS**

123 Elemental analyses involved ICP–sector field-MS (ICP–SFMS; Element XR, Thermo

Fisher Scientific, Bremen, Germany) with a 193-nm ArF Resonetics Resolution M-50 LA system, at the State Key Laboratory of Isotope Geochemistry, Guangzhou Institute of Geochemistry, Chinese Academy of Sciences (SKLaBIG-CAS), Guangzhou, China. The laser beam diameter was 33 μm, frequency 6 Hz, and energy density ~4 $J \cdot cm^{-2}$, and each spot analysis included 20 s background collection and 30 s sample signal detection. All detected major and trace element signals were normalized to ^{29}Si, using concentration data acquired by EPMA prior to LA–ICP–MS analysis (as described in supplementary information). This allowed active correction for drift, matrix effects, and fluctuations in ablation parameters. US Geological Survey basaltic glass standards GSD-1G, BCR-2G, and BHVO-2G were used as calibration standards. Molecular oxide interference was estimated as <0.3% using the $^{238}U^{16}O/^{238}U$ ratio. Experimental and data reduction techniques have been described previously by Zhang et al. (2019). Ten analyses of another basaltic glass standard TB-1G, treated as an unknown, indicated that most elemental results are within ±8% of reference values, with an analytical precision (2RSD) of better than ±10%. To visualize elemental distributions in the altered glass grain, two-dimensional elemental imaging by LA–ICP–MS was undertaken using an array of 14 × 12 spots at 33 μm intervals. The total acquisition time required for imaging was ~4 h. Data were processed by a self-developed Excel program, and elemental images (in concentration units) constructed using Surfer software.

2.2.2 Oxygen isotope and H_2O analyses by SIMS

144 Oxygen isotope ratios and H_2O concentrations were determined *in situ* using a
145 CAMECA IMS 1280-HR ion microprobe at the SKLaBIG-CAS. Instrumental parameters
146 and sample preparation techniques have been described previously by Xia et al. (2019),
147 and are summarized as follows. The primary Cs^+ ion-beam current was 3–5 nA, and a
148 normal-incidence electron-flood gun was used to compensate for sample charge.
149 Pre-sputtering (30 s) to remove the gold coating covered an area of 30 μm diameter,
150 larger than the 15 μm diameter analyzed area. A contrast aperture of 400 μm and field
151 aperture of 5000 × 5000 μm were applied. The ^{16}O, ^{18}O, and $^{16}O^1H$ ions were collected
152 simultaneously in two off-axis Faraday cups (L`2 and H1) with mass resolutions (full
153 width at half maximum, FWHM) of 2400 and one electron multiplier (FC2) with a
154 FWHM of 7000 (to avoid interference of ^{17}O). The sample and standards were mounted
155 in a Sn-based alloy mount and then stored in a vacuum oven and in SIMS ultra-vacuum
156 storage several days before performing analyses, which aims at ensuring the vacuum of
157 the instrument and reducing the interfere deriving from background.
158 Matrix effects are common in O isotope analysis of glass by SIMS (Eiler et al. 1997;
159 Hartley et al. 2012; Ickert et al. 2008), so the reference basaltic glasses BCR-2G ($\delta^{18}O$ =
160 +7.01‰), BHVO-2G ($\delta^{18}O$ = +5.60‰), BIR-1G ($\delta^{18}O$ = +5.00‰) (Hartley et al. 2012),
161 and GSD-1G were analyzed before natural samples to determine the relationship between
162 instrumental mass fractionation (IMF) and matrix composition (SiO_2 content). The $\delta^{18}O$
163 values of GSD-1G and bulk palagonite were also determined by traditional laser

fluorination GSMS. Profile analyses of the altered grain involved scanning from the core of basaltic glass to the palagonite, with analysis spots as shown in Fig. 2a. H_2O contents were calibrated by a series of glass reference materials reported by Li et al. (2015b) (supplementary Fig. 1). Oxygen isotopic compositions relative to Vienna Standard Mean Ocean Water (VSMOW; $^{18}O/^{16}O_{V\text{-}SMOW}$ = 0.0020052) and IMF corrections were calculated as follows (Baertschi 1976; Yang et al. 2018):

$$\delta^{18}O_m = (((^{18}O/^{16}O_m)/(^{18}O/^{16}O_{V\text{-}SMOW}) - 1) \times 1000 \quad (1)$$

$$IMF = \delta^{18}O_m - \delta^{18}O_{actual} \quad (2)$$

where $^{18}O/^{16}O_m$ is the raw ratio measured by SIMS, and $\delta^{18}O_m$ and $\delta^{18}O_{actual}$ are measured and recommended or corrected values, respectively.

3. Results

Two-dimensional spatial elemental distributions within a cross-section of the altered basaltic glass grain were recorded by elemental imaging using LA–ICP–MS (Figs 3, 4 and 5). Individual patterns for each element indicate that alteration did not change the chemical compositions stoichiometrically. The images indicate that the glass became depleted in major elements Ca, Al, and Na, trace elements P, Mn, Sr, V, Ba, and Co, and rare-earth elements (REE) during alteration to palagonite, and the distribution patterns of K, Rb, Li, Ni, and B mirrored or were negatively correlated with those of the former elements. The most striking observation is that major elements Fe, Ti, and Mg and trace

184 elements U, Th, Pb, Cr, Sc, Ta, Nb, Zr, Hf, and Cu are not characterized by different
185 monotonic gradients from the remnant glass core to the altered margin, with their most
186 enriched or depleted areas being limited to the vicinity of the interface between glass and
187 palagonite. The average elemental contents of glass and palagonite, and their degrees of
188 enrichment or depletion, are provided in Table 1, with the greatest depletion occurring for
189 Ca, P, V, Y, and La, with >90% loss during palagonitization, and the greatest enrichment
190 (>500%) for Li, B, K, and Rb.

191 Oxygen isotope analyses of basaltic glass standards by SIMS indicate that IMF
192 depends on SiO_2 content (Fig. 6a), so oxygen isotopic profile analyses from grain core to
193 palagonite rim (Fig. 6b) were corrected for IMF, giving the core section a uniform $\delta^{18}O$
194 value. The palagonite, however, has a distinctly higher $\delta^{18}O$ than the glass, mirroring the
195 offset in H_2O content (Fig. 6b).

196

197 **4. Discussion**

198 **4.1 Redistribution of elements during palagonitization**

199 Previous analysis of elemental flux resulting from glass palagonitization has focused
200 mainly on elemental compositions in relation to an assumed glass–palagonite immobile
201 element such as Fe, Ti, Al, or Zr (Crovisier et al. 1992; Gi Young and Sohn 2011;
202 Staudigel and Hart 1983; Utzmann et al. 2002). However, actual immobility is
203 questionable, and mobility may change during the alteration process (Knowles et al. 2013;

Stroncik and Schmincke 2001; Thorseth et al. 1991). The natural alteration environment is complex and variable, so magnitudes and directions of chemical changes during alteration, as estimated by such methods, are likely to have appreciable uncertainties. Undistorted primary textures and tight contact between glass and palagonite suggest that replacement of glass by palagonite involves little, if any, change in volume. Glass alteration is thus an isovolumetric process, as indicated by previous studies (Hay and Iijima 1968; Staudigel and Hart 1983; Stroncik and Schmincke 2001). Therefore, the chemical flux during alteration may be evaluated by a density correction of the alteration product (palagonite) based on that of basaltic glass:

$$c`_{i\,(p)} = (\rho_p/\rho_g) \times c_{i\,(p)} \quad (3)$$

where $c_{i\,(p)}$ and $c_i`_{(p)}$ are the contents of element *i* in palagonite, as directly measured by LA–ICP–MS and calculated by correction of the density difference between palagonite and basaltic glass, respectively, and ρ_p and ρ_g are the density of palagonite and basaltic glass, respectively. The values of ρ_p and ρ_g, determined by a liquid-filled pycnometer reported by Hay and Iijima (1968), are 2.56 ($2\sigma = 0.1$) and 2.19 ($2\sigma = 0.1$) $g \cdot cm^{-3}$, respectively. All elemental data for palagonite, including elemental imaging, were corrected using this method (density correction).

The elemental distribution coefficient (D) between basaltic glass and palagonite may be used to evaluate the extent of gain or loss of element during palagonitization. D>1 means gain of element and D<1 means loss of element from alteration system.

$$D_i = c_i`_{(p)} / c_{i\,(g)} \quad (4)$$

where D_i is the distribution coefficient of element *i*, and $c_{i\,(g)}$ is the content of element *i* in basaltic glass.

4.1.1 Major element distribution patterns

Average major element contents of palagonite measured by LA–ICP–MS, excluding the interface, are very similar to those determined by EPMA (Table 1 and supplementary Table 1), indicating that matrix effects between basaltic glass and palagonite in LA–ICP–MS analyses were negligible. Mapping for Na_2O, CaO, and MgO (Fig. 3b, c, d) show that their contents are lower in palagonite than in parental glass, indicating they were easily mobilized and released into pore water during alteration. Their patterns are consistent with those of previous analyses of altered sub-seafloor basaltic glasses, which indicate pronounced exchange between glass and pore water, causing depletion in Na, Ca, and Mg (Staudigel and Hart 1983; Stroncik and Schmincke 2002; Walton et al. 2005). The roles of these elements as glass silicate network modifiers and their small hydration energies may cause their high mobilities and early ion exchange with H^+ or H_3O^+ in pore water (Belza et al. 2015; Petit et al. 1990b; Robinet et al. 2006). Magnesium has the lowest concentration near the glass–palagonite interface, notably different from Na and Ca, possibly due to the incorporation of $Mg(OH)_2$ and/or scavenging of Mg from pore water during the subsequent aging and maturing of palagonite (Alt 1995; Seyfried Jr and Mottl

1982; Utzmann et al. 2002), which leads to slight enrichment in Mg relative to early palagonite. This process could be regarded as post-palagonitization, representing the continuing evolution of initial precipitation (early palagonite) towards a thermodynamically more stable layer (aging palagonite). However, Na and Ca show no such effect, implying the adsorption site in palagonite is more basic and suitable for Mg, with its hydroxide being less soluble than Na and Ca (supplementary Fig. 2).

Although K is also an alkali metal, the K_2O distribution displays an opposite trend to that of Na_2O, with enrichment in the palagonite (Fig. 3e) at a level of ~900% (Table 1). Palagonite is thus a major sink for K, with an ability to trap K released during glass dissolution and to scavenge additional K from pore water. This might be related to K being preferentially incorporated into interlayer positions of palagonite, for it is regarded as a possible precursor of smecities featuring the same behavior under submarine conditions of low temperature and high K content (Ghiara et al. 1993; Staudigel and Hart 1983), which is unlike high-temperature alteration or subaerial weathering where losses of K occur during palagonitization (Furnes 1978; Hay and Iijima 1968).

Aluminum, as a glass network-forming element, was previously regarded as being immobile during alteration in natural waters at near-neutral pH (Crovisier et al. 1992; Furnes 1978; Reesman et al. 1969), but the Al_2O_3 image (Fig. 3f) indicates otherwise, with a significant change in content from the glass–palagonite. Its distribution may be explained by the rupture of aluminate linkages because of a coordination change (from

This is the peer-reviewed, final accepted version for American Mineralogist, published by the Mineralogical Society of America.
The published version is subject to change. Cite as Authors (Year) Title. American Mineralogist, in press.
DOI: https://doi.org/10.2138/am-2021-7831. http://www.minsocam.org/

tetrahedral to octahedral Al) after exchange of glass modifier cations with aqueous H^+/H_3O^+, with the resulting six-coordinated Al species being released to solution (Casey et al. 1988; Hellmann 1995; Hellmann et al. 1990; Tsomaia et al. 2003). The Al released in highly alkaline alteration conditions (e.g., pH ≥ 10.4) which could be achieved in the alteration interface solution through ion-exchange between glass network-modifiers and solution H^+, as in this case, could be further transformed to soluble $Al(OH)_4^-$ from undissolved $Al(OH)_3$ (Hay and Iijima 1968; Jercinovic et al. 1990). The distribution of the other formative element, Si, is not discussed here, because of its use as the internal standard element in LA–ICP–MS analyses, but the SiO_2 profile analyses by EPMA (Fig. 4) indicates a trend similar to that of Al, with relative depletion in palagonite due to dissolution of the glass during palagonitization, and with highly basic conditions promoting its dissolution and mobility (Gi Young and Sohn 2011).

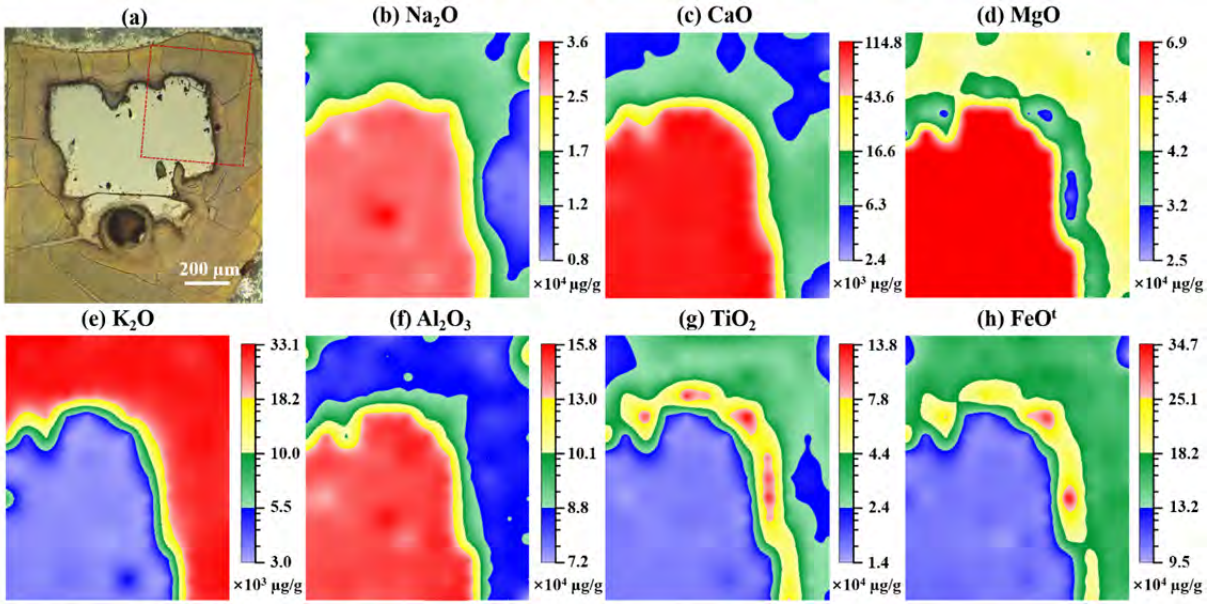

Fig. 3 (a) Photomicrograph of altered basaltic glass and LA–ICP–MS major elemental imaging of the area (0.46 × 0.40 mm), marked by the red rectangle, for (b) Na_2O, (c) CaO, (d) MgO, (e) K_2O, (f) Al_2O_3, (g) TiO_2 and (h) FeO^t (total iron oxides). Color keys indicate the logarithm of concentration.

Iron and titanium were formerly regarded as the most immobile major elements during alteration (Ailin-Pyzik and Sommer 1981; Drief and Schiffman 2004; Furnes 1978; Furnes 1984; Knowles et al. 2013; Thorseth et al. 1991; Walton et al. 2005). However, in this study, palagonite was enriched in FeO^t and TiO_2 relative to glass. In particular, the ~30 μm interface between glass and palagonite showed significant enrichment (Fig. 3g, h and Fig. 2b), distinctly different from that observed by Crovisier et al. (2003) and Pauly et al. (2011), who detected no concentration gradient from the interior to exterior of the altered rim. The unique distributions of these elements could be attributable to progressive passive accumulation, with the most soluble elements being removed from the reaction interface by dissolution. Although reduced ferrous (Fe^{2+}) iron derived from the parent glass is soluble, it could be rapidly oxidized to the less soluble Fe^{3+} (Belza et al. 2015; Knowles et al. 2013). In addition to this endogenous passive accumulation, significant exogenous Fe and Ti were also introduced into the interface. It could be deduced from the distinctly different enrichment of Fe and Ti in the interface with about 3 and 8 times compared with glass, respectively, because if it was not the case, the only

This is the peer-reviewed, final accepted version for American Mineralogist, published by the Mineralogical Society of America.
The published version is subject to change. Cite as Authors (Year) Title. American Mineralogist, in press.
DOI: https://doi.org/10.2138/am-2021-7831. http://www.minsocam.org/

298 passive accumulation should result in similar enrichment for Ti and Fe, but no such case
299 happens. The alteration-interface solution would therefore be increasingly enriched in
300 low solubility components, and then Fe–Ti oxyhydroxides would firstly and quickly
301 reach the supersaturation and precipitate (Crovisier et al. 1992; Petit et al. 1990b).
302 However, during subsequent reactions, such as the precipitation of other more soluble
303 compositions or the adsorption effect of the initial palagonite, the concentration of Fe and
304 Ti would be diluted and decrease. The Fe and Ti contents in the aging palagonite would
305 thus be lower than those in the interface vicinity, but still higher than in the former glass,
306 giving the "jump" distribution in the transition zone between basaltic glass and aging
307 palagonite. Another possibility involves the remobilization of these relatively insoluble
308 compositions or their redistribution from inner to outer zone (Furnes 1984; Gin et al.
309 2015a).

310

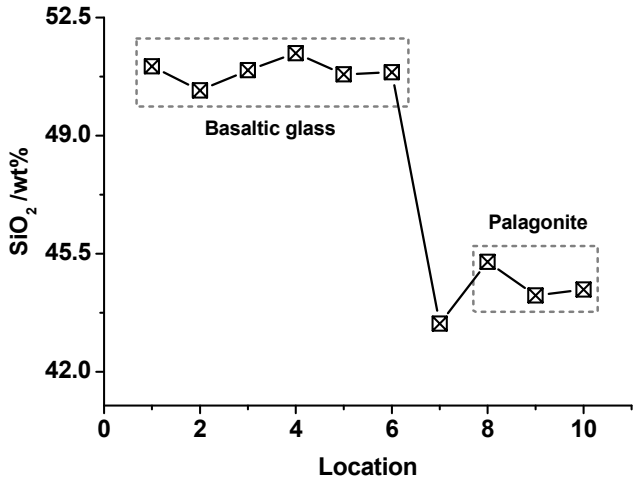

311

312 Fig. 4 SiO_2 profile from core (left, low number spots) to rim of altered glass, as

313 determined by EPMA. The spot 7 is basically on the interface. Palagonite values are
314 density-corrected as per Eq. (3). "Location" = spot number (Fig. 2a). Analytical
315 uncertainties were about ±2.5% (1σ).
316

317 **4.1.2 Trace element distribution patterns**

318 There have been many studies of changes in major element compositions, but
319 relatively few of trace element patterns during glass alteration (Berger et al. 1994;
320 Crovisier et al. 1987; Crovisier et al. 1983; Furnes 1978; Ghiara et al. 1993). Quantitative
321 elemental mapping of altered glass allows the direct examination of the mobilization of
322 trace elements during glass dissolution and precipitation of secondary phases. Only two
323 mapping studies of altered glass have been reported to date, and they were based on
324 qualitative methods with limited analysis of trace elements (Belza et al. 2015; Utzmann et
325 al. 2002).

326 The alkali metals Li and Rb have distribution characteristics similar to those of K, with
327 marked enrichment in palagonite (Figs 3e and 5a, b). This is attributed to the different
328 free energies of hydration of alkali metal ions, with the decrease in absolute values from
329 Li^+ to Rb^+ resulting in increasing preferential palagonite uptake of Li–Rb (i.e., with
330 increasing distribution coefficients) (Berger et al. 1988; Staudigel and Hart 1983) (Table
331 1). However, alkali metal ions are the predominant silicate network modifiers. When
332 glass is subjected to hydration (initial alteration), alkali metal ions are largely leached

(Petit et al. 1990b), particularly Na^+ as it is the primary network modifier in basaltic glass, and is more prevalent than Li, K, or Rb. However, when palagonite (during its precipitation) scavenges network-modifiers from pore water, where Li, K, and Rb are more abundant than in the glass, the ratio of Na^+ to other alkali metals in palagonite decreases, effectively resulting in depletion in Na and enrichment in Li, K, and Rb (Figs 3b, e and 5a, b; Table 1).

The trace alkaline earth metals Sr and Ba (Fig. 5c, d; Table 1), which have patterns similar to those of Ca, are effectively removed from the glass during alteration because of their mobility. Previous studies of altered samples based on bulk Sr isotope analyses determined that Sr in the altered phase is derived from both basaltic glass and seawater (Hart et al. 1974; Menzies and Seyfried 1979). These elements are thus depleted in palagonite, and their final concentration reflects the total budget of the exchange reaction between basaltic glass and pore water, with a significant fraction of the basaltic composition having been leached out.

Vanadium and cobalt might become soluble through formation of VO_4^{3-} and CoO_2^- (rather than insoluble $V(OH)_4$ and $Co(OH)_3$) under highly alkaline alteration conditions and behave similarly to Al, as both are depleted during alteration to palagonite (Fig. 5e, f). The mobilities of Mn (Fig. 5g) and Fe are sensitive to redox conditions, and their different distribution patterns may be attributable to the higher redox potentials of Mn, resulting in greater mobility of Mn relative to Fe (Haese 2000; Utzmann et al. 2002).

353 Another possibility is the incompatible nature of these trace elements in palagonite,
354 which would lead to a strong preference for them to enter solution.

355 Boron displays marked enrichment patterns during alteration (Fig. 5h; Table 1), owing
356 to its ability to substitute for Si in tetrahedral sites and being adsorbed in exchangeable
357 sites of palagonite (Pauly et al. 2014). Cu, Ni, and Zn are also strongly enriched in
358 palagonite (Fig. 5i and supplementary Fig. 3a, b), with a net flux of these elements from
359 seawater to the alteration phase, possibly due to their ability to easily exchange for Mg or
360 Ca (Petit et al. 1990a), or the adsorption capacity of metal oxides. Manganese oxides, for
361 example, although they have a net loss during alteration of glass, have a high adsorption
362 capacity for the cations Ni^{2+}, Cu^{2+}, and Zn^{2+} (Glasby 2006; Utzmann et al. 2002). As
363 adsorption is a surface effect, the retained elements should be restricted to the outer rim
364 of the grain, but our images indicate distributions throughout the entire palagonite layer
365 (Fig. 5i–k), indicating the effect of the porosity of palagonite (Cailleteau et al. 2008;
366 Deruelle et al. 2000).

367 The elements Pb, Cr, Sc, Hf, Zr, Ta, Th, Nb and U (in order of relative enrichment)
368 (Fig. 5j–m and supplementary Fig. 3 c–g) have behaviors paralleling those of Fe and Ti
369 (Fig. 3f, g), as they are similarly enriched in the alteration product (Table 1), especially
370 near the glass–palagonite interface where their highest content occurs. Their distributions
371 indicate relatively strong enrichment during early-stage palagonitization, with insoluble
372 "nuggets" of Fe–Ti-rich phases hosting most of these trace elements, although their

373 spatial distributions cannot be resolved by spot analyses. Their behaviors may relate to
374 the field strength of cations. These HFSE were immobile during the aqueous alteration
375 process due to their high affinities and adsorption potential for the palagonite gel material
376 (Belza et al. 2015; Petit et al. 1990b; Utzmann et al. 2002). These effects may be
377 enhanced in the interface zone, the precursor of aged palagonite, where there is greater
378 porosity (supplementary Fig. 4b) and more negatively charged surface sites than in aged
379 palagonite. Localized differences in pH may also account for their distribution and
380 enrichment within a single grain.

381 The REE imaging (Fig. 5o, p and supplementary Fig. 3h–t) indicates that the alteration
382 of glass to palagonite is accompanied by a loss of REE to hydrous solution, which is in
383 contrast to previous findings from a lake environment where they were relatively
384 enriched in palagonite because of the enhanced adsorption properties of colloids (Daux et
385 al. 1994; Jercinovic et al. 1990). This is consistent with observations of Belza et al. (2015)
386 and Staudigel and Hart (1983) that REE become remarkably depleted during glass
387 alteration. Their depletion may be due to the solubility of lanthanides being controlled
388 mainly by the availability of complex-forming ligands such as OH^-, CO_3^{2-}, and PO_4^{3-}
389 (Guy et al. 1999; Ridley 2010; Wood 1990). The anomalous depletion of highly charged
390 P^{5+} (Fig. 5n) may reflect its incorporation into a soluble complex anion such as PO_4^{3-}
391 (Walton et al. 2005), becoming a soluble chelate with the lanthanides (Gin et al. 2017;
392 Walton et al. 2005).

This is the peer-reviewed, final accepted version for American Mineralogist, published by the Mineralogical Society of America.
The published version is subject to change. Cite as Authors (Year) Title. American Mineralogist, in press.
DOI: https://doi.org/10.2138/am-2021-7831. http://www.minsocam.org/

393 In summary, four patterns of elemental distribution can be distinguished with (1)
394 strong depletion (D < 0.1; e.g., Ca, P, V, Y, and La); (2) slight depletion (1 > D > 0.1;
395 e.g., Na, Mg, Al, Si, Sr, Ba, and REE); (3) slight enrichment (2 > D > 1; e.g., Fe, Ti, Cr,
396 HFSE, Ni, Cu, and Zn); and (4) strong enrichment (D > 2; e.g., Li, B, K, and Rb) during
397 alteration.

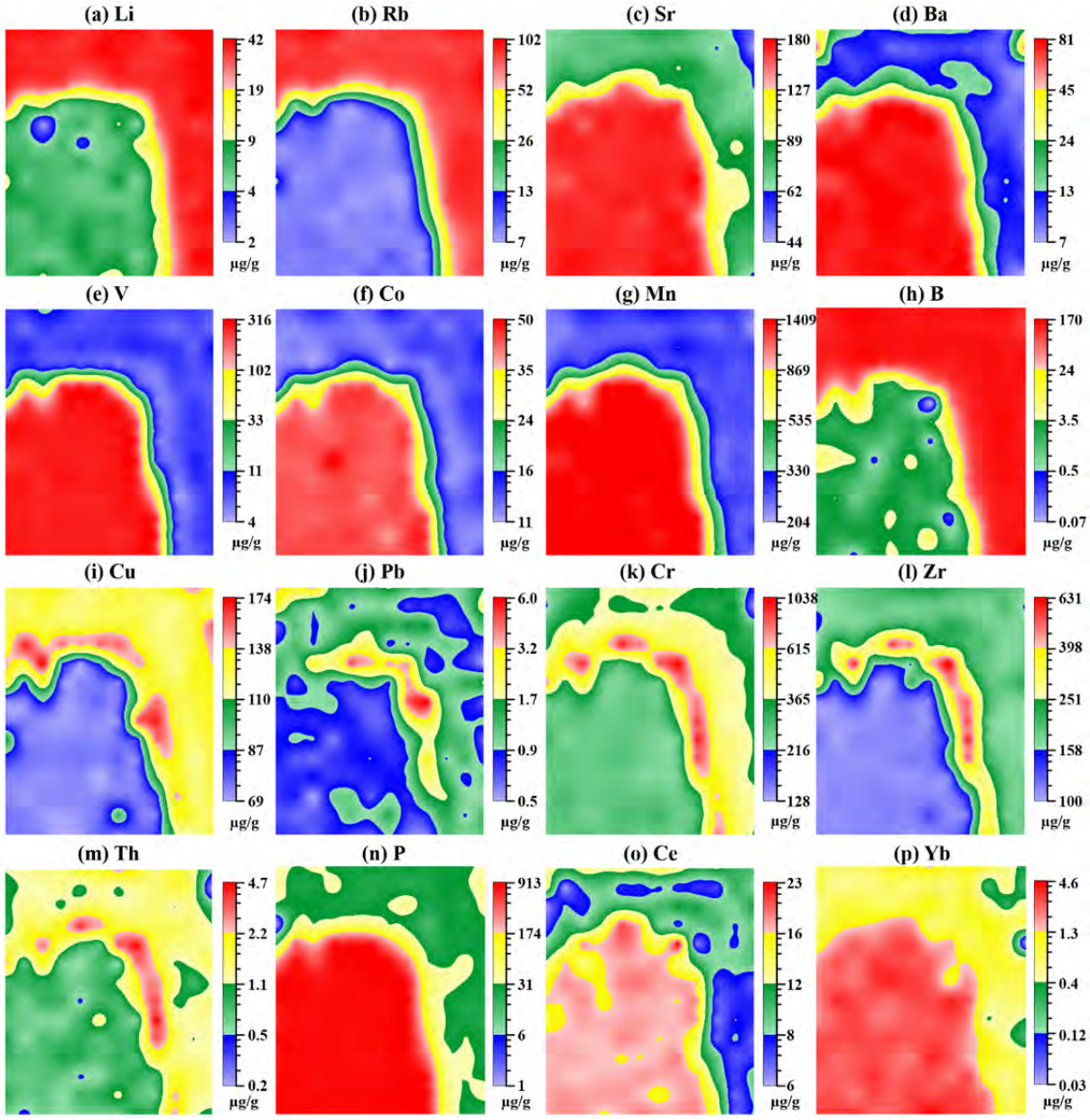

398

This is the peer-reviewed, final accepted version for American Mineralogist, published by the Mineralogical Society of America.
The published version is subject to change. Cite as Authors (Year) Title. American Mineralogist, in press.
DOI: https://doi.org/10.2138/am-2021-7831. http://www.minsocam.org/

399 Fig. 5 Trace element imaging for (a) Li, (b) Rb, (c) Sr, (d) Ba, (e) V, (f) Co, (g) Mn, (h) B,
400 (i) Cu, (j) Pb, (k) Cr, (l) Zr, (m) Th, (n) P, (o) Ce, and (p) Yb. Color keys indicate the
401 logarithm of concentration.

402

403

404

405 Table 1. Average element contents and distribution coefficients for basaltic glass and
406 palagonite, including data from LA–ICP–MS imaging, but excluding data for the glass–
407 palagonite interface and outliers.

Elements	palagonite		basaltic glass		D_i
	content	σ	content	σ	
Na_2O wt%	1.25	0.22	2.96	0.04	0.42
MgO wt%	4.40	0.06	7.35	0.02	0.60
Al_2O_3 wt%	8.61	0.08	14.65	0.02	0.59
SiO_2 wt%	44.65	0.01	51.00	0.01	0.88
K_2O wt%	3.05	0.05	0.34	0.03	9.00
CaO wt%	0.68	0.21	10.09	0.03	0.07
TiO_2 wt%	2.84	0.19	1.60	0.03	1.78
FeO wt%	15.96	0.08	10.47	0.02	1.52
Li ppm	36.80	0.09	6.27	0.15	5.63
B ppm	137.87	0.10	2.79	0.32	46.63
P ppm	28.30	0.31	830.73	0.02	0.03
Sc ppm	51.11	0.10	32.44	0.05	1.58
V ppm	6.92	0.21	265.87	0.03	0.03
Cr ppm	375.84	0.17	255.56	0.05	1.47
Mn ppm	267.24	0.09	1403.20	0.02	0.19
Co ppm	13.44	0.08	42.90	0.04	0.31
Ni ppm	186.34	0.09	116.56	0.04	1.60
Cu ppm	126.60	0.08	72.90	0.03	1.74
Zn ppm	112.17	0.12	85.85	0.05	1.31
Rb ppm	83.39	0.08	7.85	0.05	10.62
Sr ppm	75.91	0.13	167.58	0.03	0.45
Y ppm	2.77	0.29	29.52	0.03	0.09

Zr ppm	187.26	0.12	113.07	0.03	1.66
Nb ppm	14.59	0.25	8.12	0.04	1.80
Ba ppm	13.28	0.66	76.35	0.05	0.17
La ppm	0.43	0.38	7.09	0.06	0.06
Ce ppm	9.16	0.23	17.38	0.05	0.53
Pr ppm	0.34	0.37	2.40	0.06	0.14
Nd ppm	1.76	0.45	11.89	0.10	0.15
Sm ppm	0.88	0.52	3.67	0.13	0.24
Eu ppm	0.33	0.41	1.34	0.15	0.25
Gd ppm	1.09	0.37	4.91	0.10	0.22
Tb ppm	0.25	0.43	0.75	0.14	0.33
Dy ppm	1.54	0.34	4.95	0.12	0.31
Ho ppm	0.26	0.37	1.03	0.12	0.25
Er ppm	0.79	0.47	3.09	0.20	0.26
Tm ppm	0.12	0.43	0.40	0.20	0.29
Yb ppm	0.76	0.39	2.82	0.17	0.27
Lu ppm	0.08	0.56	0.41	0.24	0.19
Hf ppm	4.32	0.17	2.64	0.19	1.63
Ta ppm	0.78	0.14	0.45	0.29	1.73
Pb ppm	1.19	0.45	0.88	0.60	1.35
Th ppm	1.31	0.27	0.73	0.23	1.79
U ppm	0.36	0.23	0.19	0.23	1.88

4.2 Oxygen isotope and H_2O profiles during palagonitization

Analyses of glass oxygen isotopes by SIMS are sensitive to matrix effects, as shown in Fig. 6a and consistent with previous studies (Eiler et al. 1997; Gurenko and Chaussidon 2002; Hartley et al. 2012; Ickert et al. 2008). Oxygen isotopic profiles from grain core to palagonite rim indicate a uniform core $\delta^{18}O$ value of +6.01‰ ± 0.25‰ (2σ; spots 1–6; Fig. 6b) within the range of MORB glass (5.3‰–6.2‰) (Eiler 2001; Ito et al. 1987). This indicates that the grain core is less influenced by alteration, and still represents fresh basaltic glass, consistent with the minor variation in elemental contents within the core

417 (Table 1; Figs 3 and 5). The palagonite (spots 7–10; Fig. 6b), however, is strongly
418 enriched in ^{18}O ($\delta^{18}O$ = +21.3‰ to +22.3‰), with the average SIMS $\delta^{18}O$ value being
419 consistent with that determined by laser fluorination (+21.80‰ ± 0.24‰; 2σ; n = 3). The
420 matrix effect on SIMS oxygen isotope analyses between basaltic glass and palagonite is
421 thus negligible under the instrumental conditions used. Oxygen atoms are located mainly
422 within the glass tetrahedral silicate network (Garlick and Dymond 1970; Geisler et al.
423 2010), and cannot be displaced by exogenous oxygen in the core because of a lack of
424 dissolution–reprecipitation. However, the notably different $\delta^{18}O$ values of palagonite
425 indicate that exogenous ^{18}O from interstitial fluid or other sources is incorporated into the
426 silica network of palagonite, either by glass dissolution–reprecipitation or by palagonite
427 hydrolysis-recondensation (Gin et al. 2018; Gin et al. 2015a).

428 The H_2O content of glass and palagonite are usually calculated by assuming that its
429 concentration equals the difference between 100% and the total of oxides determined by
430 EPMA analyses (Pauly et al. 2011; Utzmann et al. 2002; Walton et al. 2005), with
431 possible overestimation as the minor and trace element compositions are included in the
432 total. Here, *in situ* H_2O contents of altered basaltic glass were determined directly by
433 SIMS, and resulting values were around half those calculated by the indirect EPMA
434 method in both parental glass and palagonite. The H_2O profile from grain core to rim
435 indicates a trend similar to that of $\delta^{18}O$, with the core having a uniform H_2O content of
436 0.43 wt.% ± 0.01% (2σ; spots 1–6; Fig. 6b), increasing to 3.72 wt.% ± 0.14% (2σ; spots

437 7–10; Fig 6b) in the palagonite. Palagonite thus has a much higher water content than
438 basaltic glass, consistent with the alteration reaction requiring significant amounts of
439 water (Furnes 1978; Pauly et al. 2011; Staudigel and Hart 1983; Stroncik and Schmincke
440 2002). However, palagonite water contents measured here are lower than those reported
441 previously (Furnes 1978; Pauly et al. 2011; Staudigel and Hart 1983). This may be
442 attributed to the presence of two forms of water in palagonite, namely combined water
443 (H_3O^+, resulting from hydration of glass) and adsorbed water (H_2O^-, related only to the
444 rock porosity) (Furnes 1978). The latter may be present in larger amounts, but is easier to
445 remove as it is located mainly on larger-scale palagonite features such as vesicles and
446 fractures. Our sample was stored in a vacuum oven and in SIMS ultra-vacuum storage
447 before analyses, and the adsorbed water might have escaped, resulting in a lower
448 measured water content. Furthermore, compositional and crystallinity variations in
449 palagonite are factors that cannot be ignored (Pauly et al. 2011).
450

This is the peer-reviewed, final accepted version for American Mineralogist, published by the Mineralogical Society of America.
The published version is subject to change. Cite as Authors (Year) Title. American Mineralogist, in press.
DOI: https://doi.org/10.2138/am-2021-7831. http://www.minsocam.org/

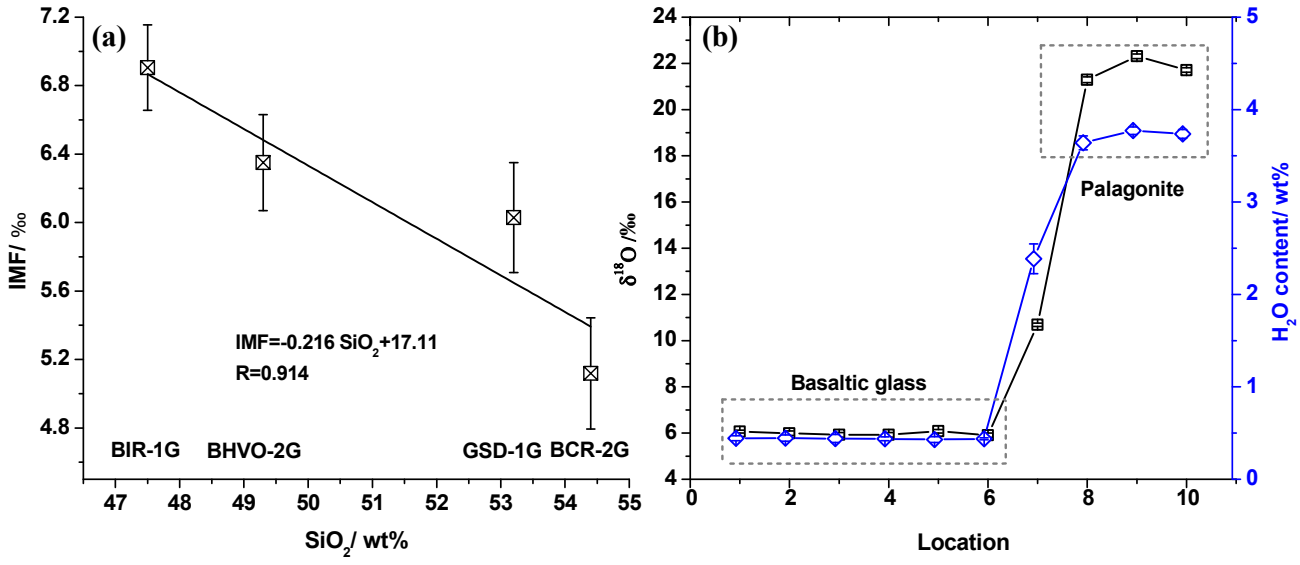

Fig. 6 (a) Instrumental mass fractionation (IMF) vs. SiO_2 content, showing the linear variation in IMF with respect to chemical compositions of reference materials in the SIMS oxygen isotope analysis of basaltic glass, where the $\delta^{18}O_{actual}$ of GSD-1G (9.64‰ ± 0.43‰; 2σ) was first determined by laser fluorination. Error bars represent 2σ of 15 SIMS analyses. (b) Oxygen isotopic and H_2O content profiles from core to rim of altered glass, (analysis-spot locations as in Fig. 2a). Error bars represent 1σ.

4.3 Alteration process for submarine basaltic glass

Mechanisms proposed for the alteration of glass include hydration and ion exchange, hydrolysis of the silicate network, condensation–reprecipitation and dissolution–reprecipitation (Crovisier et al. 2003; Drief and Schiffman 2004; Frugier et al. 2008; Geisler et al. 2010; Gin et al. 2016; Hellmann et al. 2012; Ojovan et al. 2006; Putnis and Putnis 2007; Putnis et al. 2007; Stroncik and Schmincke 2002; Techer et al. 2000; Techer et al. 2001a). Dissolution–reprecipitation has become the generally accepted model for

alteration of basaltic glass to palagonite (Berger et al. 1987; Crovisier et al. 1987; Daux et al. 1994; Drief and Schiffman 2004; Hellmann et al. 2012; Jercinovic et al. 1990; Techer et al. 2001b), but the question remains as to whether the dissolution is congruent or incongruent. Congruent dissolution could be readily identified in experimental studies by monitoring elemental releases from glass to aqueous solution (Crovisier et al. 1987). Incongruent dissolution, however, is more difficult to identify because reactions occurring on the glass surface are complex and variable (Crovisier et al. 1983; Drief and Schiffman 2004). The second remaining question is whether palagonite becomes a diffusion barrier for water and soluble elements. Comparison between mean dissolution rates and initial dissolution rate could help answer this question (Parruzot, et al. 2015). Another remaining question concerns the process of palagonitization from initial precipitation to mature palagonite.

The oxygen isotope analysis and elemental imaging of an individual grain reveal the sequential alteration from basaltic glass to palagonite. The sharp and distinct chemical compositional changes at the evidently delimited interface (where the finer processes revealed would rely on techniques with the higher spatial resolution reported by Hellmann et al. (2015) and Gin et al (2013, 2017)) between pristine glass and palagonite may indicate that palagonite was formed through reprecipitation on the surface of remnant glass after congruent dissolution of the glass network, rather than by simple hydration and devitrification. This is supported by the difference in physical morphology

485 between glass and palagonite. Incongruent dissolution would result in a sponge-like
486 surface structure of dissolving materials, whereas congruent dissolution would form a
487 smooth and undistorted surface (Stroncik and Schmincke 2001); the morphological
488 features of the analyzed palagonite (Fig. 2) suggest the latter.

489 Based on the variations in elemental and oxygen isotopic compositions, and the
490 morphological features between basaltic glass and palagonite, three reaction stages are
491 suggested for the process of submarine basaltic glass alteration (Fig. 7): (1) ion exchange
492 and formation of a leached layer; (2) congruent dissolution and precipitation; and (3)
493 post-palagonitization.

494 In stage (1), elements in the glass might be selectively leached by ion exchange with
495 pore water H_3O^+ or H^+, with the most leached species being network-modifier cations
496 such as Na^+, Mg^{2+}, and Ca^{2+}, owing to their high solubility and relatively weak $–SiO^–$ (or
497 $–AlO^–$) bonds (Petit et al. 1990b), resulting in the formation of a superficial leached layer.
498 The thickness of this layer might be in the range of nanometers (Gi Young and Sohn
499 2011; Gin et al. 2017; Gin et al. 2013; Hellmann et al. 2015; Thorseth et al. 1991), and
500 could not be resolved by laser sampling. However, its presence cannot be precluded,
501 because it is difficult to directly disrupt the silicate network of the basaltic glass under
502 alteration conditions involving the near-neutral pH (pH = ~7.2) of pore water and low
503 temperatures (Li et al. 2015a).

504 After stage (1), the interface solution pH would increase with predominant transport of

505 H_3O^+ or H^+ into the glass and ion exchange with network-modifier cations. Stage (2)
506 commences when the pH exceeds 9 and the glass Si–O tetrahedral network is destroyed
507 (Dran et al. 1988; Gin et al. 2015b; Petit et al. 1990b; Robinet et al. 2006) (Fig. 4). The
508 pH is then much higher than that of surrounding pore water, with the reaction solution
509 being separated from pore water (to maintain such a difference while avoiding dilution)
510 (Crovisier et al. 2003; Gi Young and Sohn 2011; Lee et al. 2006; Ojovan et al. 2006;
511 Robinet et al. 2006) in a semi-closed environment. If completely closed, it would be
512 expected that compositional gradients from the outermost palagonite toward the interior
513 (later-formed) portions would occur (Jercinovic et al. 1990), but no such effects were
514 observed. Either covering by subsequent formation of palagonite rims (possibly a thin
515 innermost film within it), or polymerization of dissolved orthosilicic acid would obstruct
516 fluid pathways and lower fluid flow-rates (Belza et al. 2015; Crovisier et al. 2003; Geisler
517 et al. 2010; Gin et al. 2018; Parruzot et al. 2015; Techer et al. 2001; Utzmann et al. 2002),
518 forming a more closed alteration system, whose barrier effects can also be ascertained
519 from the residual rate (mean value is 1.6×10^{-7} $g.m^{-2}.d^{-1}$) which is approximately five
520 orders of magnitudes lower than the initial alteration rate (about 1.75×10^{-2} $g.m^{-2}.d^{-1}$,
521 T=4°C, extrapolated from Parruzot et al. (2015)). During stage (2), the outer leached
522 layer would be dissolved congruently, with Ti^{4+}, Fe^{3+} (from oxidized Fe^{2+}), and most
523 HFSE (Zr, Nb, Sc, Hf, Th, and Ta) being the first to reach the solubility limits of their
524 hydroxides and precipitating on the outermost glass surface, almost simultaneously with

its congruent dissolution. The partial loss of non-modifiers such as Al, P, and REE would also occur in this stage. Although the reaction interface is gradually separated from pore water by increasing thickness of palagonite, the nanometer-sized porosity of the palagonite (supplementary Fig. 4) may provide diffusion pathways for dissolved elements to escape to solution, with elements such as Fe, Ti, and HFSE being scavenged from some other source or passively enriched (Cailleteau et al. 2008; Deruelle et al. 2000; Gin et al. 2011; Hellmann et al. 2012; Kerisit and Liu 2009; Pauly et al. 2011; Tsomaia et al. 2003; Utzmann et al. 2002).

In stage (3) (post-palagonitization), the growing palagonite would incorporate additional species such as $Mg(OH)_2$ (Jercinovic et al. 1990), and the initial porous palagonite may continue to evolve to a state of quasi-equilibrium with surrounding solution (Belza et al. 2015; Pauly et al. 2011; Putnis 2009; Putnis et al. 2005), with the composition of aging palagonite being slightly modified in the process.

The alteration model proposed here (Fig. 7) describes the alteration of basaltic glass to palagonite under submarine conditions, focusing on initial precipitation and the evolution to mature palagonite before the crystallization phase, possibly providing insight into the alteration of oceanic crust. We have characterized major and trace element and isotopic patterns during palagonitization, whereas most previous studies have reported mechanisms that focus more on leaching processes in confined media, and over short timescales in laboratory-based simulation experiments (Crovisier et al. 2003; Gin et al.

This is the peer-reviewed, final accepted version for American Mineralogist, published by the Mineralogical Society of America.
The published version is subject to change. Cite as Authors (Year) Title. American Mineralogist, in press.
DOI: https://doi.org/10.2138/am-2021-7831. http://www.minsocam.org/

2017; Gin et al. 2015a; Gin et al. 2015b; Gin et al. 2013; Hellmann et al. 2012; Ojovan et al. 2006; Parruzot et al. 2015; Putnis et al. 2007; Techer et al. 2000; Techer et al. 2001a). Such conditions are significantly different to those of natural alteration, especially in long-term submarine environments where aqueous chemistry is much more complex, and involves free metal cations, ligand complexing agents, humic substances, and organic and inorganic acids (Drever 2005). Furthermore, alteration processes and their corresponding elemental features are strongly influenced by the composition and structure of the parental glass, temperature, pH, and the composition of the alteration solution (Bunker 1994; Crovisier et al. 2003; Gin et al. 2012; Gin et al. 2015b; Gin et al. 2016; Hellmann et al. 2012; Ojovan et al. 2006; Parruzot et al. 2015; Stroncik and Schmincke 2002; Utzmann et al. 2002).

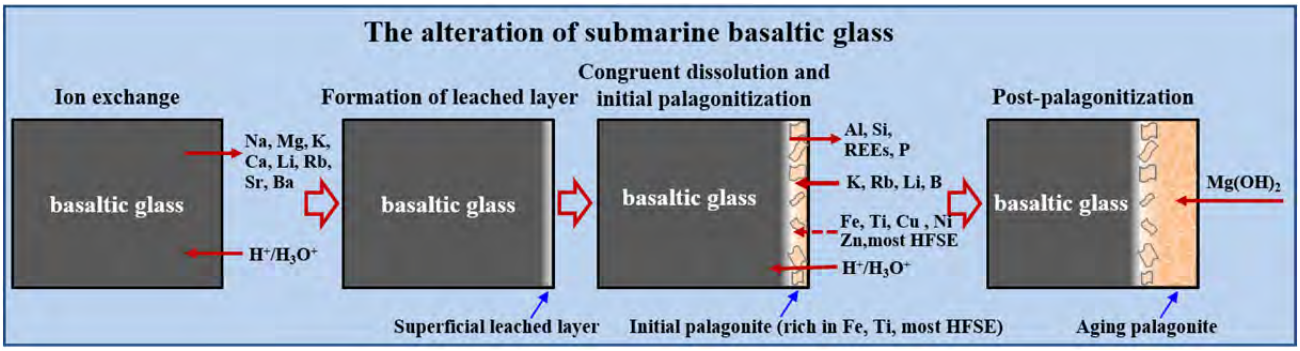

Fig. 7 Possible alteration processes for submarine basaltic glass, where the inferred process of ion exchange and formation of the leached layer is based on previous studies (Belza et al. 2015; Boksay et al. 1968; Crovisier et al. 2003; Ducasse et al. 2018; Gin et al. 2017; Gin et al. 2015b; Gin et al. 2016; Gin et al. 2013; Techer et al. 2000; Techer et al. 2001b).

562

563 **4. Implication**

564 LA–ICP–MS elemental imaging and SIMS oxygen isotopic analysis on a
565 submarine-altered basaltic glass specimen provide distribution patterns of major and trace
566 elements and $\delta^{18}O$ values from the glass to the palagonite (alteration product). Different
567 elements exhibit different behaviors during alteration, and are either added from pore
568 water or removed during alteration. Geochemical distribution patterns from the glass to
569 the glass–palagonite interface and then to the palagonite rim indicate multiple reaction
570 stages, involving selective leaching and formation of a leached layer, congruent
571 dissolution and initial precipitation, and palagonite maturation. Directions and intensities
572 of chemical fluxes vary within the individual grain, and may provide insight into
573 geochemical cycles and the mechanisms of palagonite formation during oceanic crust
574 alteration.

575 **Acknowledgement**

576 The English of the manuscript was improved by Stallard Scientific Editing. This work
577 was supported by the National Natural Sciences Foundation of China (41991325 and
578 41803010), the GIGCAS 135 Project (135PY201605), the Guangzhou Institute of
579 Geochemistry (TGC201804) and the State Key Laboratory of Isotope Geochemistry
580 (SKLaBIG-JY-19-04). The data for this paper are available on Zenodo
581 (doi.org/10.5281/zenodo.3786289). The authors have no conflict of interest to declare.

582 This is contribution IS-XXXX from GIGCAS.

583

584 **References**

585 Ailin-Pyzik, I., and Sommer, S. (1981) Microscale chemical effects of low temperature
586 alteration of DSDP basaltic glasses. Journal of Geophysical Research: Solid Earth,
587 86(B10), 9503-9510.

588 Alt, J.C. (1995) Subseafloor processes in mid-ocean ridge hydrothermal systems.
589 Geophysical Monograph Series, 91, 85-114.

590 Baertschi, P. (1976) Absolute ^{18}O content of standard mean ocean water. Earth &
591 Planetary Science Letters, 31(3), 341–344.

592 Belza, J., Goderis, S., Smit, J., Vanhaecke, F., Baert, K., Terryn, H., and Claeys, P. (2015)
593 High spatial resolution geochemistry and textural characteristics of 'microtektite'
594 glass spherules in proximal Cretaceous–Paleogene sections: Insights into glass
595 alteration patterns and precursor melt lithologies. Geochimica et Cosmochimica
596 Acta, 152, 1-38.

597 Berger, G., Claparols, C., Guy, C., and Daux, V. (1994) Dissolution rate of a basalt glass
598 in silica-rich solutions: implications for long-term alteration. Geochimica et
599 Cosmochimica Acta, 58(22), 4875-4886.

600 Berger, G., Schott, J., and Guy, C. (1988) Behavior of Li, Rb and Cs during basalt glass
601 and olivine dissolution and chlorite, smectite and zeolite precipitation from

602 seawater: Experimental investigations and modelization between 50° and 300°C.
603 Chemical Geology, 71(4), 297-312.
604 Berger, G., Schott, J., and Loubet, M. (1987) Fundamental processes controlling the first
605 stage of alteration of a basalt glass by seawater: an experimental study between
606 200° and 320°C. Earth & Planetary Science Letters, 84(4), 431-445.
607 Boksay, Z., Bouquet, G., and Dobos, S. (1968) Kinetics of the formation of leached
608 layers on glass surfaces. Physics and Chemistry of Glasses, 9(2), 69-71.
609 Bunker, B.C. (1994) Molecular mechanisms for corrosion of silica and silicate glasses.
610 Journal of Non-Crystalline Solids, 179, 300–308.
611 Cailleteau, C., Angeli, F., Devreux, F., Gin, S., Jestin, J., Jollivet, P., and Spalla, O. (2008)
612 Insight into silicate-glass corrosion mechanisms. Nature Materials, 7(12), 978–
613 983.
614 Casey, W.H., Westrich, H.R., and Arnold, G.W. (1988) Surface chemistry of labradorite
615 feldspar reacted with aqueous solutions at pH = 2, 3, and 12. Geochimica et
616 Cosmochimica Acta, 52(12), 2795-2807.
617 Crovisier, J.L., Advocat, T., and Dussossoy, J.L. (2003) Nature and role of natural
618 alteration gels formed on the surface of ancient volcanic glasses (Natural analogs
619 of waste containment glasses). Journal of Nuclear Materials, 321(1), 91-109.
620 Crovisier, J.L., Honnorez, J., and Eberhart, J.P. (1987) Dissolution of basaltic glass in
621 seawater: Mechanism and rate. Geochimica et Cosmochimica Acta, 51(11),

622 2977-2990.

623 Crovisier, J.L., Honnorez, J., Fritz, B., and Petit, J.C. (1992) Dissolution of subglacial
624 volcanic glasses from Iceland: laboratory study and modelling. Applied
625 Geochemistry, 7, 55-81.

626 Crovisier, J.L., Thomassin, J.H., Juteau, T., Eberhart, J.P., Touray, J.C., and Baillif, P.
627 (1983) Experimental seawater-basaltic glass interaction at 50°C: Study of early
628 developed phases by electron microscopy and X-ray photoelectron spectrometry.
629 Geochimica et Cosmochimica Acta, 47(3), 377-387.

630 Daux, V., Crovisier, J., Hemond, C., and Petit, J. (1994) Geochemical evolution of
631 basaltic rocks subjected to weathering: fate of the major elements, rare earth
632 elements, and thorium. Geochimica et Cosmochimica Acta, 58(22), 4941-4954.

633 Deruelle, O., Spalla, O., Barboux, P., and Lambard, J. (2000) Growth and ripening of
634 porous layers in water altered glasses. Journal of Non-Crystalline Solids, 261,
635 237–251.

636 Dran, J.-C., Della Mea, G., Paccagnella, A., Petit, J.-C., and Trotignon, L. (1988) The
637 aqueous dissolution of alkali silicate glasses: reappraisal of mechanisms by H and
638 Na depth profiling with high energy ion beams. Physics and Chemistry of Glasses,
639 29(6), 249-255.

640 Drever, J.I. (2005) Surface and Ground Water, Weathering, and Soils: Treatise on
641 Geochemistry, Volume 5. Elsevier.

642 Drief, A., and Schiffman, P. (2004) Very low-temperature alteration of sideromelane in
643 hyaloclastites and hyalotuffs from Kilauea and Mauna Kea volcanoes:
644 Implications for the mechanism of palagonite formation. Clays and Clay Minerals,
645 52(5), 622–634.
646 Ducasse, T., Gourgiotis, A., Pringle, E., Moynier, F., Frugier, P., Jollivet, P., and Gin, S.
647 (2018) Alteration of synthetic basaltic glass in silica saturated conditions: Analogy
648 with nuclear glass. Applied Geochemistry, 97, 19-31.
649 Eiler, J.M. (2001) Oxygen isotope variations of basaltic lavas and upper mantle rocks.
650 Reviews in Mineralogy and Geochemistry, 43, 319–364.
651 Eiler, J.M., Graham, C., and Valley, J.W. (1997) SIMS analysis of oxygen isotopes:
652 matrix effects in complex minerals and glasses. Chemical Geology, 138(3-4),
653 221–244.
654 Frugier, P., Gin, S., Minet, Y., Chave, T., Bonin, B., Godon, N., Lartigue, J.E., Jollivet, P.,
655 Ayral, A., De Windt, L., and Santarini, G. (2008) SON68 nuclear glass dissolution
656 kinetics: Current state of knowledge and basis of the new GRAAL model. Journal
657 of Nuclear Materials, 380(1), 8–21.
658 Furnes, H. (1978) Element mobility during palagonitization of a subglacial hyaloclastite
659 in Iceland. Chemical Geology, 22(3), 249-264.
660 Furnes, H. (1984) Chemical changes during progressive subaerial palagonitization of a
661 subglacial olivine tholeiite hyaloclastite: A microprobe study. Chemical Geology,

662 43(3-4), 271-285.

663 Garlick, G.D., and Dymond, J.R. (1970) Oxygen Isotope Exchange between Volcanic
664 Materials and Ocean Water. Geological Society of America Bulletin, 81(7), 2137–
665 2142.

666 Geisler, T., Janssen, A., Scheiter, D., Stephan, T., Berndt, J., and Putnis, A. (2010)
667 Aqueous corrosion of borosilicate glass under acidic conditions: A new corrosion
668 mechanism. Journal of Non-Crystalline Solids, 356(28), 1458–1465.

669 Ghiara, M.R., Franco, E., Petti, C., Stanzione, D., and Valentino, G.M. (1993)
670 Hydrothermal interaction between basaltic glass, deionized water and seawater.
671 Chemical Geology, 104(1–4), 125-138.

672 Gi Young, J., and Sohn, Y.K. (2011) Microtextures, microchemistry, and mineralogy of
673 basaltic glass alteration, Jeju Island, Korea, with implications for elemental
674 behavior. American Mineralogist, 96(7), 1129–1147.

675 Gin, S., Beaudoux, X., Angéli, F., Jégou, C., and Godon, N. (2012) Effect of composition
676 on the short-term and long-term dissolution rates of ten borosilicate glasses of
677 increasing complexity from 3 to 30 oxides. Journal of Non-Crystalline Solids,
678 358(18), 2559-2570.

679 Gin, S., Collin, M., Jollivet, P., and Fournier, M. (2018) Dynamics of self-reorganization
680 explains passivation of silicate glasses. Nature Communications, 9(1), 2169.

681 Gin, S., Guittonneau, C., Godon, N., Neff, D., Rebiscoul, D., Cabié, M., and Mostefaoui,

682 S. (2011) Nuclear glass durability: new insight into alteration layer properties.
683 The Journal of Physical Chemistry C, 115(38), 18696-18706.
684 Gin, S., Jollivet, P., Barba Rossa, G., Tribet, M., Mougnaud, S., Collin, M., Fournier, M.,
685 Cadel, E., Cabie, M., and Dupuy, L. (2017) Atom-Probe Tomography, TEM and
686 ToF-SIMS study of borosilicate glass alteration rim: A multiscale approach to
687 investigating rate-limiting mechanisms. Geochimica et Cosmochimica Acta, 202,
688 57-76.
689 Gin, S., Jollivet, P., Fournier, M., Angeli, F., Frugier, P., and Charpentier, T. (2015a)
690 Origin and consequences of silicate glass passivation by surface layers. Nature
691 Communications, 6, 6360.
692 Gin, S., Jollivet, P., Fournier, M., Berthon, C., Wang, Z., Mitroshkov, A., Zhu, Z., and
693 Ryan, J.V. (2015b) The fate of silicon during glass corrosion under alkaline
694 conditions: a mechanistic and kinetic study with the international simple glass.
695 Geochimica et Cosmochimica Acta, 151, 68-85.
696 Gin, S., Neill, L., Fournier, M., Frugier, P., Ducasse, T., Tribet, M., Abdelouas, A.,
697 Parruzot, B., Neeway, J., and Wall, N. (2016) The controversial role of
698 inter-diffusion in glass alteration. Chemical Geology, 440, 115-123.
699 Gin, S., Ryan, J.V., Schreiber, D.K., Neeway, J., and Cabié, M. (2013) Contribution of
700 atom-probe tomography to a better understanding of glass alteration mechanisms:
701 Application to a nuclear glass specimen altered 25 years in a granitic environment.

Chemical Geology, 349, 99-109.

Gislason, S.R., and Eugster, H.P. (1987) Meteoric water-basalt interactions. II: A field study in NE Iceland. Geochimica et Cosmochimica Acta, 51(10), 2841-2855.

Glasby, G.P. (2006) Manganese: Predominant Role of Nodules and Crusts. Marine Geochemistry, 371-427.

Grambow, B., Jercinovic, M., Ewing, R., and Byers, C. (1985) Weathered basalt glass: a natural analogue for the effects of reaction progress on nuclear waste glass alteration. Mater. Res. Soc. Symp. Proc., 50.

Gurenko, A.A., and Chaussidon, M. (2002) Oxygen isotope variations in primitive tholeiites of Iceland: evidence from a SIMS study of glass inclusions, olivine phenocrysts and pillow rim glasses. Earth & Planetary Science Letters, 205(1), 63–79.

Guy, C., Daux, V., and Schott, J. (1999) Behaviour of rare earth elements during seawater/basalt interactions in the Mururoa Massif. Chemical Geology, 158(1–2), 21-35.

Haese, R.R. (2000) The reactivity of iron. Marine geochemistry, p. 233-261. Springer.

Hart, R. (1970) Chemical exchange between sea water and deep ocean basalts. Earth & Planetary Science Letters, 9(3), 269-279.

Hart, S. (1969) K, Rb, Cs contents and K/Rb, K/Cs ratios of fresh and altered submarine basalts. Earth & Planetary Science Letters, 6(4), 295-303.

722 Hart, S., Erlank, A., and Kable, E. (1974) Sea floor basalt alteration: some chemical and
723 Sr isotopic effects. Contributions to Mineralogy and Petrology, 44(3), 219-230.
724 Hartley, M.E., Thordarson, T., Taylor, C., Fitton, J.G., and Eimf. (2012) Evaluation of the
725 effects of composition on instrumental mass fractionation during SIMS oxygen
726 isotope analyses of glasses. Chemical Geology, 334, 312–323.
727 Hay, R.L., and Iijima, A. (1968) Nature and origin of palagonite tuffs of the Honolulu
728 group on Oahu, Hawaii. Geological Society of America Memoirs, 116, 331-76.
729 Hellmann, R. (1995) The albite-water system: Part II. The time-evolution of the
730 stoichiometry of dissolution as a function of pH at 100, 200, and 300°C.
731 Geochimica et Cosmochimica Acta, 59(9), 1669-1697.
732 Hellmann, R., Cotte, S., Cadel, E., Malladi, S., Karlsson, L.S., Lozano-Perez, S., Cabié,
733 M., and Seyeux, A. (2015) Nanometre-scale evidence for interfacial dissolution–
734 reprecipitation control of silicate glass corrosion. Nature Materials, 14(3), 307.
735 Hellmann, R., Eggleston, C.M., Hochella Jr, M.F., and Crerar, D.A. (1990) The formation
736 of leached layers on albite surfaces during dissolution under hydrothermal
737 conditions. Geochimica et Cosmochimica Acta, 54(5), 1267-1281.
738 Hellmann, R., Wirth, R., Daval, D., Barnes, J.-P., Penisson, J.-M., Tisserand, D., Epicier,
739 T., Florin, B., and Hervig, R.L. (2012) Unifying natural and laboratory chemical
740 weathering with interfacial dissolution–reprecipitation: A study based on the
741 nanometer-scale chemistry of fluid–silicate interfaces. Chemical Geology,

294-295, 203-216.

Ickert, R., Hiess, J., Williams, I., Holden, P., Ireland, T., Lanc, P., Schram, N., Foster, J., and Clement, S. (2008) Determining high precision, in situ, oxygen isotope ratios with a SHRIMP II: analyses of MPI-DING silicate-glass reference materials and zircon from contrasting granites. Chemical Geology, 257(1-2), 114–128.

Ito, E., White, W.M., and Göpel, C. (1987) The O, Sr, Nd and Pb isotope geochemistry of MORB. Chemical Geology, 62(3), 157–176.

Jantzen, C., and Plodinec, M. (1984) Thermodynamic model of natural, medieval and nuclear waste glass durability. Journal of Non-Crystalline Solids, 67(1-3), 207-223.

Jercinovic, M.J., Keil, K., Smith, M.R., and Schmitt, R.A. (1990) Alteration of basaltic glasses from north-central British Columbia, Canada. Geochimica et Cosmochimica Acta, 54(10), 2679-2696.

Kerisit, S., and Liu, C. (2009) Molecular Simulations of Water and Ion Diffusion in Nanosized Mineral Fractures. Environmental Science & Technology, 43(3), 777-782.

Knowles, E., Staudigel, H., and Templeton, A. (2013) Geochemical characterization of tubular alteration features in subseafloor basalt glass. Earth & Planetary Science Letters, 374(6), 239-250.

Lee, W.E., Ojovan, M.I., Stennett, M.C., and Hyatt, N.C. (2006) Immobilization of

762 radioactive waste in glasses, glass composite materials and ceramics. Advances in
763 Applied Ceramics, 105(1), 3–12.
764 Li, C.-F., Lin, J., Kulhanek, D., Williams, T., Bao, R., Briais, A., Brown, E., Chen, Y.,
765 Clift, P., and Colwell, F. (2015a) Expedition 349 summary.
766 Li, C.-F., Xu, X., Lin, J., Sun, Z., Zhu, J., Yao, Y., Zhao, X., Liu, Q., Kulhanek, D.K.,
767 Wang, J., Song, T., Zhao, J., Qiu, N., Guan, Y., Zhou, Z., Williams, T., Bao, R.,
768 Briais, A., Brown, E.A., Chen, Y., Clift, P.D., Colwell, F.S., Dadd, K.A., Ding, W.,
769 Almeida, I.H., Huang, X.-L., Hyun, S., Jiang, T., Koppers, A.A.P., Li, Q., Liu, C.,
770 Liu, Z., Nagai, R.H., Peleo-Alampay, A., Su, X., Tejada, M.L.G., Trinh, H.S., Yeh,
771 Y.-C., Zhang, C., Zhang, F., and Zhang, G.-L. (2014) Ages and magnetic
772 structures of the South China Sea constrained by deep tow magnetic surveys and
773 IODP Expedition 349. Geochemistry Geophysics Geosystems, 15(12),
774 4958-4983.
775 Li, Y., Dasgupta, R., and Tsuno, K. (2015b) The effects of sulfur, silicon, water, and
776 oxygen fugacity on carbon solubility and partitioning in Fe-rich alloy and silicate
777 melt systems at 3 GPa and 1600 °C: Implications for core–mantle differentiation
778 and degassing of magma oceans and reduced planetary mantles. Earth &
779 Planetary Science Letters, 415, 54-66.
780 Lutze, W., Malow, G., Ewing, R., Jercinovic, M., and Keil, K. (1985) Alteration of basalt
781 glasses: implications for modelling the long-term stability of nuclear waste

782 glasses. Nature, 314(6008), 252-255.

783 Menzies, M., and Seyfried, W.E. (1979) Basalt-seawater interaction: trace element and
784 strontium isotopic variations in experimentally altered glassy basalt. Earth &
785 Planetary Science Letters, 44(3), 463-472.

786 Morgenstein, M., and Riley, T.J. (1974) Hydration-rind dating of basaltic glass: A new
787 method for archaeological chronologies. Asian Perspectives, 17(2), 145-159.

788 Nikitczuk, M.P.C., Schmidt, M.E., and Flemming, R.L. (2016) Candidate microbial
789 ichnofossils in continental basaltic tuffs of central Oregon, USA: expanding the
790 record of endolithic microborings. Geological Society of America Bulletin,
791 128(7/8), 1270-1285.

792 Ojovan, M.I., Pankov, A., and Lee, W.E. (2006) The ion exchange phase in corrosion of
793 nuclear waste glasses. Journal of Nuclear Materials, 358(1), 57–68.

794 Parruzot, B., Jollivet, P., Rébiscoul, D., and Gin, S. (2015) Long-term alteration of
795 basaltic glass: Mechanisms and rates. Geochimica et Cosmochimica Acta, 154,
796 28–48.

797 Pauly, B.D., Schiffman, P., Zierenberg, R.A., and Clague, D.A. (2011) Environmental and
798 chemical controls on palagonitization. Geochemistry Geophysics Geosystems,
799 12(12), doi:10.1029/2011gc003639.

800 Pauly, B.D., Williams, L.B., Hervig, R.L., Schiffman, P., and Zierenberg, R.A. (2014)
801 Methods for in situ SIMS microanalysis of Boron and its isotopes in palagonite.

802 Clays and Clay Minerals, 62(3), 224–234.

803 Petit, J.C., Mea, G.D., Dran, J.C., Magonthier, M.C., Mando, P.A., and Paccagnella, A.
804 (1990a) Hydrated-layer formation during dissolution of complex silicate glasses
805 and minerals. Geochimica et Cosmochimica Acta, 54(7), 1941-1955.

806 Petit, J.C., Mea, G.D., Dran, J.C., Magonthier, M.C., and Paccagnella, A. (1990b)
807 Hydrated-layer formation during dissolution of complex silicate glasses and
808 minerals. Geochimica et Cosmochimica Acta, 54(7), 1941-1955.

809 Putnis, A. (2009) Mineral replacement reactions. Reviews in Mineralogy and
810 Geochemistry, 70(1), 87-124.

811 Putnis, A., and Putnis, C.V. (2007) The mechanism of reequilibration of solids in the
812 presence of a fluid phase. Journal of Solid State Chemistry, 180(5), 1783-1786.

813 Putnis, C.V., Geisler, T., Schmid-Beurmann, P., Stephan, T., and Giampaolo, C. (2007)
814 An experimental study of the replacement of leucite by analcime. American
815 Mineralogist, 92(1), 19-26.

816 Putnis, C.V., Tsukamoto, K., and Nishimura, Y. (2005) Direct observations of
817 pseudomorphism: compositional and textural evolution at a fluid-solid interface.
818 American Mineralogist, 90(11-12), 1909-1912.

819 Reeman, A., Pickett, E., and Keller, W. (1969) Aluminum ions in aqueous solutions.
820 American Journal of Science, 267(1), 99-113.

821 Ridley, W. (2010) Petrology of associated igneous rocks in volcanogenic massive sulfide

occurrence model. US Geological Survey Scientific Investigations Report, 32.

Robinet, L., Coupry, C., Eremin, K., and Hall, C. (2006) Raman investigation of the structural changes during alteration of historic glasses by organic pollutants. Journal of Raman Spectroscopy, 37(11), 1278-1286.

Saheb, M., Loisel, C., Duhamel, R., and Remusat, L. (2015) Use of hydrogen isotopes to understand stained glass weathering. Procedia Earth and Planetary Science, 13, 64-67.

Seyfried Jr, W.E., and Mottl, M.J. (1982) Hydrothermal alteration of basalt by seawater under seawater-dominated conditions. Geochimica et Cosmochimica Acta, 46(6), 985-1002.

Staudigel, H., and Hart, S.R. (1983) Alteration of basaltic glass: Mechanisms and significance for the oceanic crust-seawater budget. Geochimica et Cosmochimica Acta, 47(3), 337–350.

Stroncik, N.A., and Schmincke, H.-U. (2002) Palagonite – a review. International Journal of Earth Sciences, 91(4), 680–697.

Stroncik, N.A., and Schmincke, H.U. (2001) Evolution of palagonite: Crystallization, chemical changes, and element budget. Geochemistry Geophysics Geosystems, 2(7), doi:10.1029/2000GC000102.

Techer, I., Advocat, T., Lancelot, J., and Liotard, J.-M. (2000) Basaltic glass: alteration mechanisms and analogy with nuclear waste glasses. Journal of Nuclear Materials,

282(1), 40-46.

Techer, I., Advocat, T., Lancelot, J., and Liotard, J.-M. (2001a) Dissolution kinetics of basaltic glasses: control by solution chemistry and protective effect of the alteration film. Chemical Geology, 176(1-4), 235-263.

Techer, I., Lancelot, J., Clauer, N., Liotard, J.M., and Advocat, T. (2001b) Alteration of a basaltic glass in an argillaceous medium: The Salagou dike of the Lodève Permian Basin (France). Analogy with an underground nuclear waste repository. Geochimica et Cosmochimica Acta, 65(7), 1071-1086.

Thorseth, I.H., Furnes, H., and Tumyr, O. (1991) A textural and chemical study of Icelandic palagonite of varied composition and its bearing on the mechanism of the glass-palagonite transformation. Geochimica et Cosmochimica Acta, 55(3), 731–749.

Tsomaia, N., Brantley, S.L., Hamilton, J.P., Pantano, C.G., and Mueller, K.T. (2003) NMR evidence for formation of octahedral and tetrahedral Al and repolymerization of the Si network during dissolution of aluminosilicate glass and crystal. American Mineralogist, 88(1), 54-67.

Utzmann, A., Hansteen, T., and Schmincke, H.U. (2002) Trace element mobility during sub-seafloor alteration of basaltic glass from Ocean Drilling Program site 953 (off Gran Canaria). International Journal of Earth Sciences, 91(4), 661-679.

Walton, A., and Schiffman, P. (2003) Alteration of hyaloclastites in the HSDP 2 Phase 1

862 Drill Core 1. Description and paragenesis. Geochemistry Geophysics Geosystems,
863 4(5), doi: 10.1029/2002GC000368.
864 Walton, A.W., Schiffman, P., and Macpherson, G. (2005) Alteration of hyaloclastites in
865 the HSDP 2 Phase 1 Drill Core: 2. Mass balance of the conversion of
866 sideromelane to palagonite and chabazite. Geochemistry Geophysics Geosystems,
867 6(9), doi: 10.1029/2004GC000903.
868 Wood, S.A. (1990) The aqueous geochemistry of the rare-earth elements and yttrium: 1.
869 Review of available low-temperature data for inorganic complexes and the
870 inorganic REE speciation of natural waters. Chemical Geology, 82, 159-186.
871 Xia, X.P., Cui, Z.X., Li, W., Zhang, W.F., Yang, Q., Hui, H., and Lai, C.K. (2019) Zircon
872 water content: reference material development and simultaneous measurement of
873 oxygen isotopes by SIMS. Journal of Analytical Atomic Spectrometry, 34(6),
874 1088-1097.
875 Yang, Q., Xia, X., Zhang, W., Zhang, Y., Xiong, B., Xu, Y., Wang, Q., and Wei, G. (2018)
876 An evaluation of precision and accuracy of SIMS oxygen isotope analysis. Solid
877 Earth Sciences, 3(3), 81–86.
878 Zhang, G.L., Luo, Q., Zhao, J., Jackson, M.G., Guo, L.S., and Zhong, L.F. (2018a)
879 Geochemical nature of sub-ridge mantle and opening dynamics of the South
880 China Sea. Earth & Planetary Science Letters, 489, 145–155.
881 Zhang, L., Ren, Z.Y., Xia, X.P., Yang, Q., Hong, L.B., and Wu, D. (2019) In situ

882 determination of trace elements in melt inclusions using laser ablation inductively
883 coupled plasma sector field mass spectrometry. Rapid Communications in Mass
884 Spectrometry, 33(4), 361-370.

885